Supplementary Materials

Table S1. Phenotype information of the subjects excluded from this study

ID	Subject	Release	Gender	Age	Exclusion criteria
1	131621	Q1	F	26-30	Uncompleted R-fMRI scans
2	144428	Q1	M	22-25	Uncompleted R-fMRI scans
3	230926	Q1	F	26-30	Uncompleted R-fMRI scans
4	235128	Q1	F	26-30	Uncompleted R-fMRI scans
5	355542	Q1	F	26-30	Uncompleted R-fMRI scans
6	611231	Q1	F	31-35	Uncompleted R-fMRI scans
7	707244	Q1	F	26-30	Uncompleted R-fMRI scans
8	733548	Q1	F	31-35	Uncompleted R-fMRI scans
9	116120	Q2	F	31-35	Uncompleted R-fMRI scans
10	207628	Q2	M	31-35	Uncompleted R-fMRI scans
11	119833	Q1	F	26-30	Missing time points in R-fMRI scans
12	150423	Q1	F	26-30	Missing time points in R-fMRI scans
13	140420	Q2	F	26-30	Missing time points in R-fMRI scans
14	103515	Q1	F	26-30	Excessive head motion
15	103818	Q1	F	31-35	Excessive head motion
16	111312	Q1	F	31-35	Excessive head motion
17	114924	Q1	M	26-30	Excessive head motion
18	117122	Q1	F	26-30	Excessive head motion
19	125525	Q1	F	31-35	Excessive head motion
20	143325	Q1	F	31-35	Excessive head motion
21	156637	Q1	M	31-35	Excessive head motion
22	191437	Q1	F	31-35	Excessive head motion
23	199150	Q1	F	26-30	Excessive head motion
24	250427	Q1	F	31-35	Excessive head motion
25	665254	Q1	F	31-35	Excessive head motion
26	901139	Q1	F	26-30	Excessive head motion
27	937160	Q1	M	26-30	Excessive head motion
28	123117	Q2	M	26-30	Excessive head motion
29	151223	Q2	F	26-30	Excessive head motion
30	175439	Q2	F	31-35	Excessive head motion
31	298051	Q2	F	31-35	Excessive head motion
32	579665	Q2	F	31-35	Excessive head motion
33	677968	Q2	F	31-35	Excessive head motion
34	702133	Q2	F	31-35	Excessive head motion
35	753251	Q2	M	26-30	Excessive head motion
36	788876	Q2	F	31-35	Excessive head motion
37	984472	Q2	F	26-30	Excessive head motion

In summary, thirty-seven subjects were excluded from the current study, including ten subjects (IDs: 1-10) with uncompleted R-fMRI scans, three subjects (IDs: 11-13) with time point missing in R-fMRI scans and twenty-four subjects (IDs: 14-37) with excessive head motion.

Figure S1

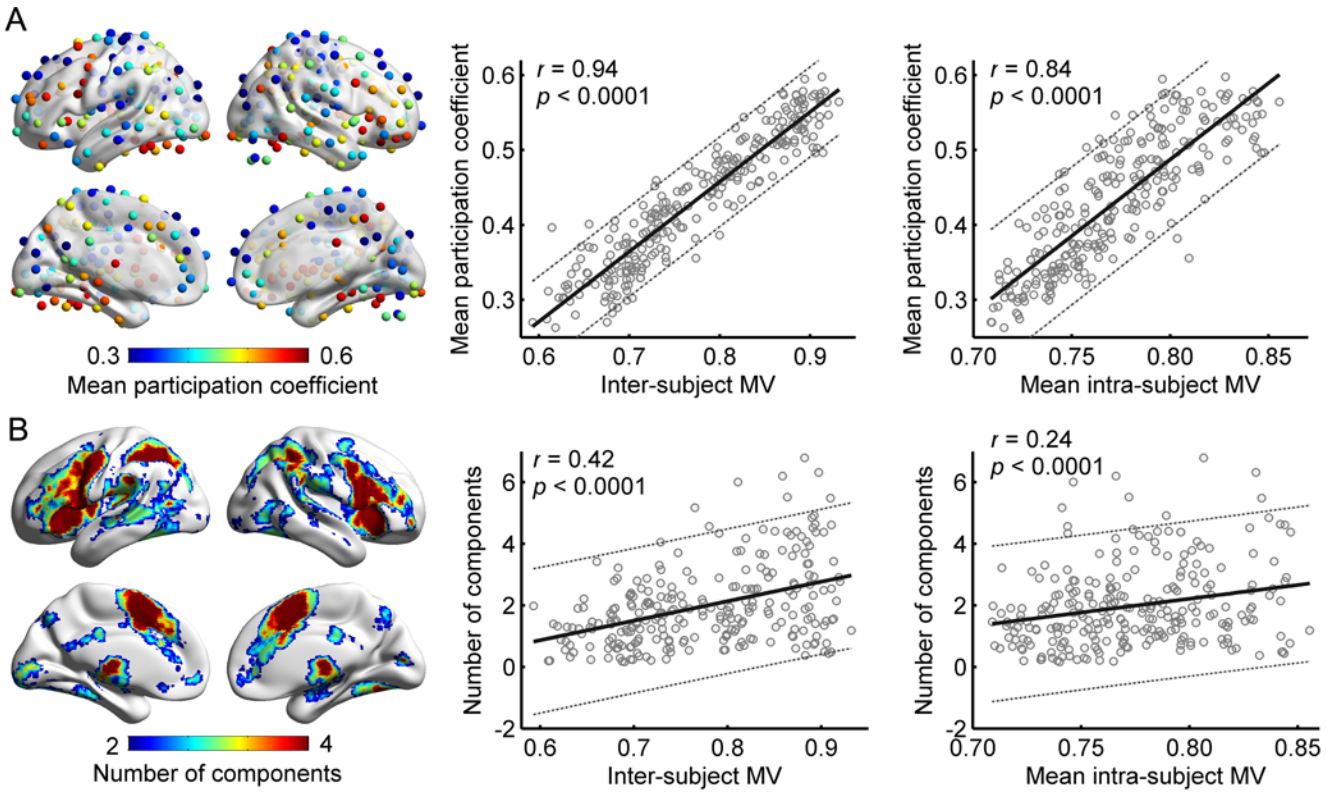

Figure S1. Relationship with participation coefficients and cognitive flexibility in Session 2. (A) Mean participation coefficient across subjects (left panel) and the across-node relationship with inter-subject modular variability (middle panel) and the mean intra-subject modular variability across subjects (right panel). (B) Number of cognitive components adapted from Yeo et al. (2015) (left panel) and the across-node relationship with inter-subject modular variability (middle panel) and the mean intra-subject modular variability across subjects (right panel). For each nodal region, we estimated its cognitive flexibility by averaging the cognitive component numbers of all voxels within this node. The dotted lines in the scatter plots denote the 95% prediction error bounds, hereinafter the same. MV, modular variability.

Figure S2

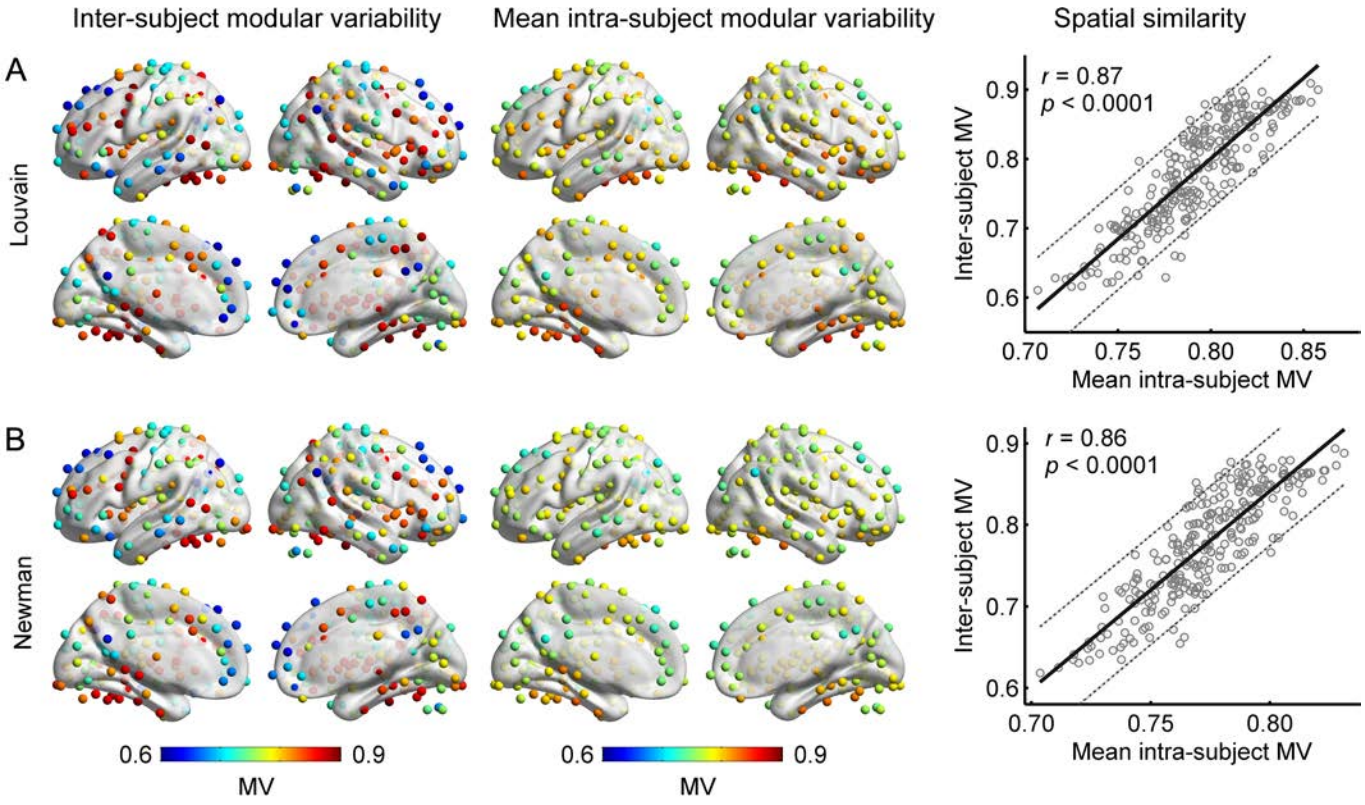

Figure S2. Inter- and mean intra-subject modular variability maps and their spatial similarity with different module detection algorithms. (A) Inter- and mean intra-subject modular variability with the functional modules detected through the Louvain algorithm (Blondel et al. 2008). (B) Inter- and mean intra-subject modular variability with the functional modules detected through the Newman algorithm (Newman 2006). All network analyses were performed on the R-fMRI data in Session 1. MV, modular variability.

Figure S3

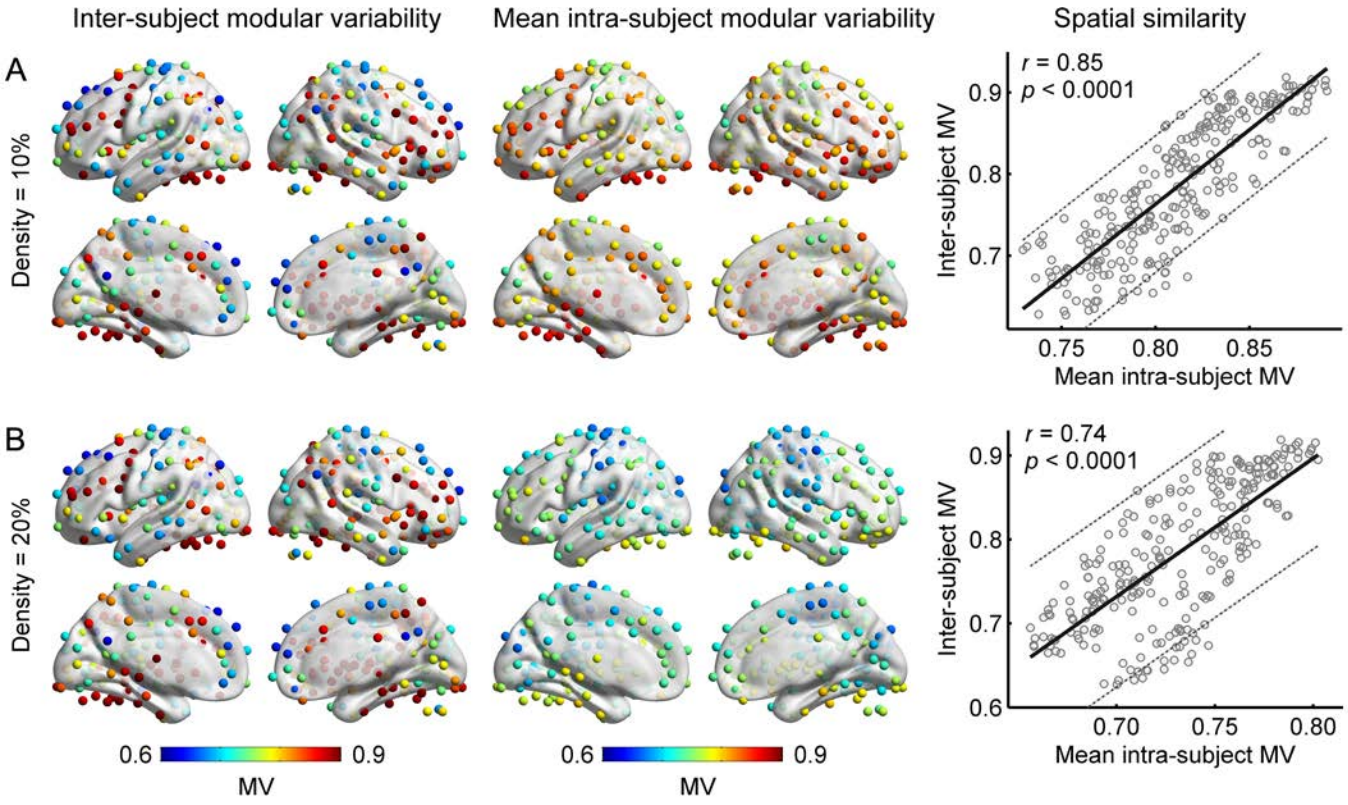

Figure S3. Inter- and mean intra-subject modular variability maps and their spatial similarity with different network densities. (A) Inter- and mean intra-subject modular variability in functional networks with a density of 10%. (B) Inter- and mean intra-subject modular variability in functional networks with a density of 20%. All network analyses were performed on the R-fMRI data in Session 1. MV, modular variability.

Figure S4

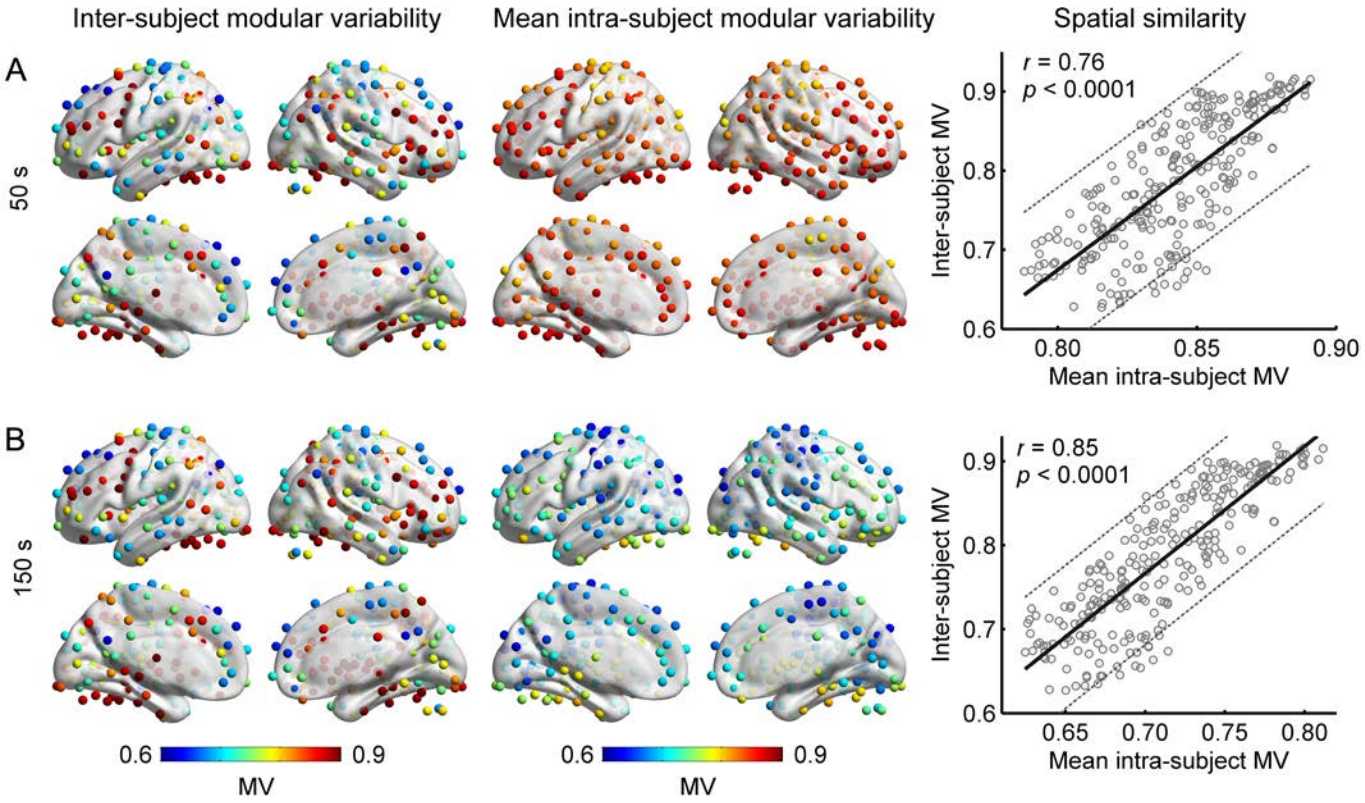

Figure S4. Inter- and mean intra-subject modular variability maps and their spatial similarity with different sliding window lengths. (A) Inter- and mean intra-subject modular variability with a sliding window length of 50 s. (B) Inter- and mean intra-subject modular variability with a sliding window length of 150 s. All network analyses were performed on the R-fMRI data in Session 1. MV, modular variability.

Figure S5

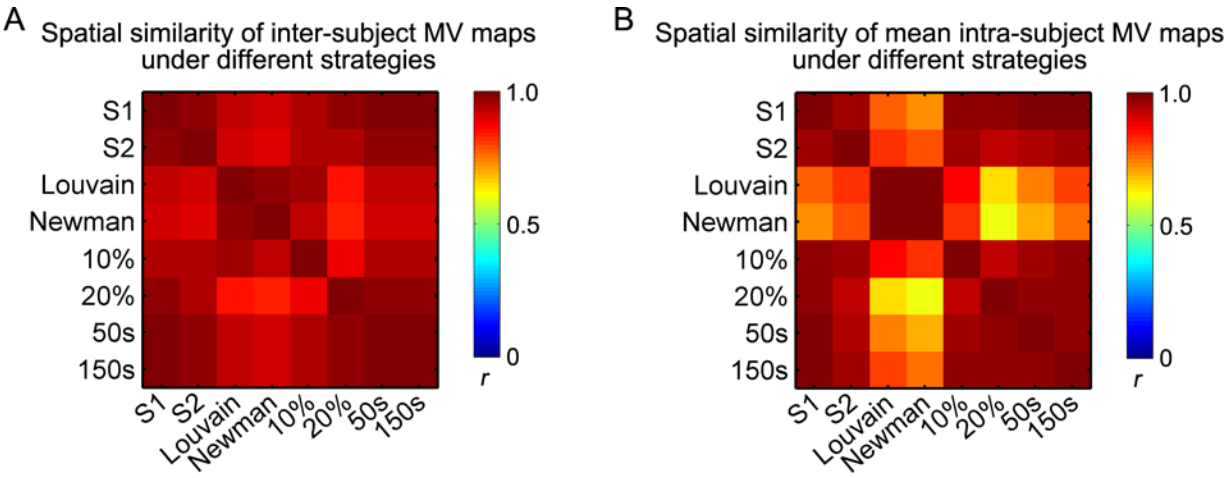

Figure S5. Reproducibility of inter-subject (A) and mean intra-subject (B) modular variability maps under different network analysis strategies. All functional networks were constructed using a functional atlas consisting of 264 nodes (Power et al., 2011) based on R-fMRI data in the first session (i.e., S1), except the strategy denoted by S2. The spatial patterns of both inter-subject and mean intra-subject modular variability were well reproducible across different strategies, as evidenced by high Pearson's correlations among strategies. MV, modular variability.

Figure S6

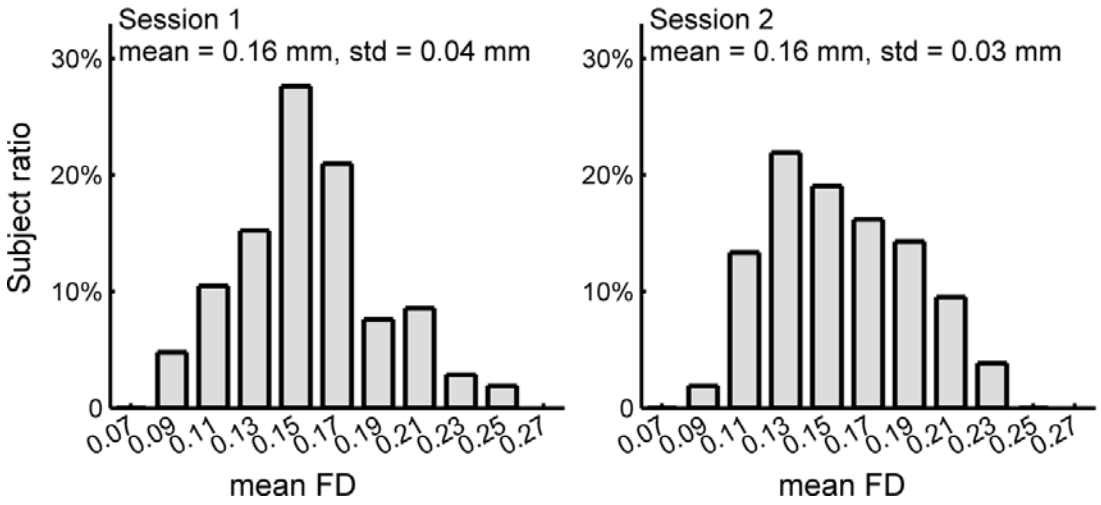

Figure S6. Normalized histograms of head motion parameters for 105 subjects used in the main analysis. For each subject in each session, we calculated the framewise displacements (FD, Power et al., 2012) for every time point and averaged them across time to obtain mean FD. For these subjects, their mean FD values showed small values in both sessions (Session 1, mean ± std = 0.16 ± 0.04 mm; Session 2, mean ± std = 0.16 ± 0.03 mm). FD, framewise displacement.

Figure S7.

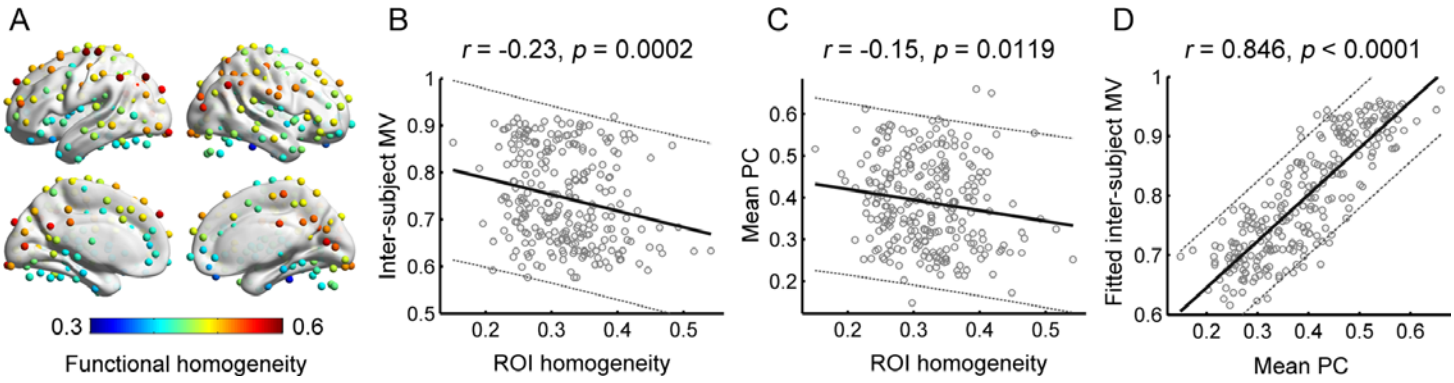

Figure S7. (A) Functional homogeneity map at the group level. (B) Across-node correlation between functional homogeneity and inter-subject modular variability. (C) Across-node correlation between functional homogeneity and mean participation coefficient across subjects. (D) Across-node correlation between inter-subject modular variability and mean participation coefficient after correcting for nodal functional homogeneity index. Notably, the spatial correlation between inter-subject modular variability and mean participation coefficient changed very little from 0.849 to 0.846 after correcting for the influence of nodal homogeneity. For each subject, functional homogeneity of a node was defined as an average temporal correlation of the mean time course of this node against the time courses of all voxels within this node. The nodal homogeneity index at the group level was obtained by averaging individual homogeneity across subjects. Of note, to reduce the potential influence of head motion, these analyses were performed on the 17 subjects with very stringent head motion control. PC, participation coefficient; MV, modular variability.

Figure S8

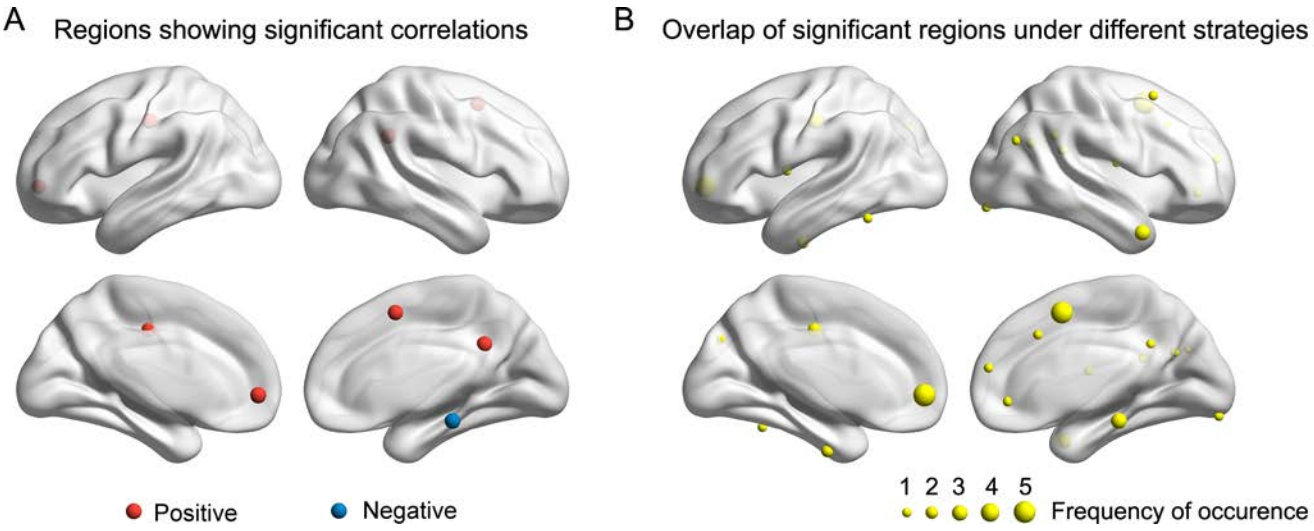

Figure S8. Brain regions showing significant correlations between regional intra-subject modular variability and individual fluid intelligence. (A) Significant regions in dynamic functional networks constructed with a network density of 15% and a sliding window length of 100 s. Red, positive correlation; Blue, negative correlation. (B) Overlap of significant brain regions across five analysis strategies, including varying network densities (10%, 15% and 20%) with a fixed sliding window length of 100 s, and varying window lengths (50 s and 150 s) with a fixed network density of 15%. Node sizes indicate the frequency of occurrence as significant regions across five strategies. In HCP data, the fluid intelligence score was measured using Raven's Progressive Matrices with 24 items. Here, we used the scores (PMAT24_A_CR) indicating the number of correct responses. The ROI-wise correlation analyses were performed between regional intra-subject modular variability and individual fluid intelligence scores across 105 subjects ($p < 0.05$, uncorrected for multiple comparisons).